

# Numerical Study on the Performance of Thermocline Tank for Hybrid Solar Tower Power Plants using DEM-CFD Coupled Method

Karem Elsayed Elfeky, Abubakar Gambo Mohammed, Qiuwang Wang\*

Key Laboratory of Thermo-Fluid Science and Engineering, MOE, Xi'an Jiaotong University, Xi'an, Shaanxi 710049, China  
[wangqw@mail.xjtu.edu.cn](mailto:wangqw@mail.xjtu.edu.cn)

Solar tower power (STP) plants integrated with thermal energy storage (TES) subsystems are expected to be a potential solution to meet the world's future energy needs. Air rock bed TES subsystem emphasizes to be efficient and cheap storage for STP plants. In the present study, the discrete element method (DEM) coupled with the computational fluid dynamics (CFD) model are adopted to study the fluid flow and heat transfer process of an air rock thermocline TES tank prototype. The study is carried out to investigate the thermal behaviour of the TES thermocline tank by changing the Reynolds number. The results demonstrated that the higher void fraction near the wall results in a lower solid mass to absorb thermal energy and the temperature in the near-wall region is much higher than in core region at low Reynolds number but with increasing the Reynolds number this temperature difference decreasing. The results show that the temperature difference between both the HTF and the spheres for charging cycle decreases with increasing of the Reynolds number, but also the total rate of heat transfer increases. The results illustrated that the difference in temperature between both the spheres and the HTF during the discharging cycle decreases with increase in the Reynolds number and this difference in temperature is less during the discharging cycle than the charging cycle.

## 1. Introduction

Solar energy is the best sources of energy expected to meet the world's energy requirements, reduce fuel prices and prevent the increase of greenhouse gases emission (Pizzolato et al., 2017). The intermittent nature of solar energy needs an energy storage subsystem to use the energy source effectively. The technologies of solar thermal energy, such as solar tower power (STP) plants; capture the thermal energy of the sun and convert it into electrical power by a heat engine connected with a generator (Pramanik and Ravikrishna, 2017). One of the most significant features of STP technology is its ability to store energy efficiently and at low cost (Li and Ju, 2018). The thermal energy storage (TES) subsystem in an air rock thermocline tank is efficient and reasonable storage for STP plants (Hoivik et al., 2019).

More recently, the subject of TES using bed rocks has been of interest to researchers. The most important properties of storage materials are the heat capacity and the conductivity, but the conductivity has less effect (Hänchen et al., 2011). The thermal behaviour of the TES thermocline tank has been investigated to know how to improve the heat transfer process during the charging/discharging cycles (Elfeky et al., 2018). The results showed that there was a significant increase in discharge efficiency and the discharge time was reduced. Rao et al. (2019) presented the performance investigation of three lab-scale solid sensible heat storage prototypes. In a similar work, Tiskatine et al. (2017) studied the effect of the axial porosity variation and how to select convenient storage medium for packed bed TES subsystem and compared the results with 3-D CFD simulations. The results demonstrated that the temperature profiles for the charging/discharging cycles and pressure drop were influenced by the axial porosity variation. The first researchers who conduct a study to determine the coefficient of heat transfer in a porous medium filled with rocks (Löf et al., 1984). The results illustrated that the rate of heat transfer depends on the mass flux and the particle size, while the inlet temperature has no obvious effect. The thermal performance of a 1 MWe STP plants has been investigated using direct and indirect TES subsystems by Cocco et al. (2015). The study revealed that the performance of two-tank TES is higher than the

thermocline TES tank, but the cost of producing energy for STP plants is reduced by using a thermocline TES tank.

Based on the above literature review, it can be noted that most of the previous numerical studies lack clear knowledge for the process of the heat transfer between the HTF and the filler material in detail, e.g., influence of the Reynolds number on the amount of increasing/decreasing the temperature of the filler material for the charging/discharging cycles and the influence of the Reynolds number on the absorb and recover thermal energy, especially at low Reynolds number during charging/discharging cycles. In the present study, the thermal performance of the random packed bed for a prototype thermocline TES tank is numerically investigated a different Reynolds number for the charging/discharging cycles. The current article describes the development of an innovative method for investigating the thermal performance of the thermocline thermal energy storage tank which used in solar tower power plants, a technology that is aimed at energy conservation, the optimal use of energy resources, the optimisation of energy processes, and sustainable energy systems.

## 2. Model formulation

### 2.1 Physical model

Packed bed TES subsystems have proven its effectiveness in the thermal storage process because of its high heat transfer rate during the charging/discharging cycles. Figure 1 schematically shows the structure of the thermocline TES tank prototype. The aspect ratio ( $H_{\text{tank}}/D_{\text{bed}}$ ) of the tank is 4.287, comparable to that used in STP applications (Zanganeh et al., 2015). The thermocline TES tank contains a vertical cylinder with two distributors, one at the inlet and the other at the outlet as shown in Figure 1. During the charging cycle, the hot HTF at temperature  $T_h$  passing from the top part of the tank, transfers energy to the spheres and exits from the bottom part. During the discharging cycle, the cold HTF passing from the bottom part of the tank at temperature  $T_c$ , collects heat from the spheres and exits from the top part. The packed bed region height is indicated by  $H_{\text{bed}}$ , while  $D_{\text{bed}}$  indicated the diameter of the tank. The thermocline TES tank is filled with 515 spheres at average porosity of  $\phi$ . The geometrical parameters of the packing models are presented in Table 1.

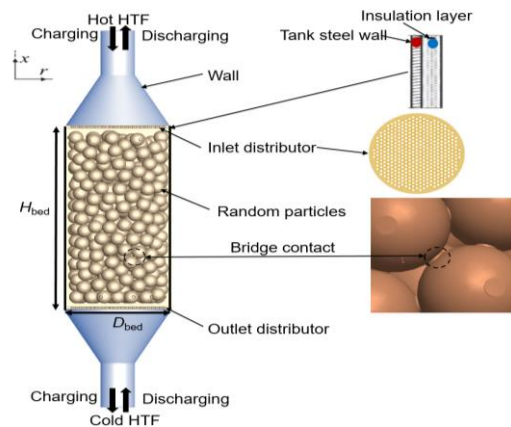


Figure 1: Schematic diagram of physical model of the thermocline TES tank

Table 1: Geometrical parameters of thermocline TES tank

Parameters	Values	Parameters	Values
$H_{\text{tank}}$ (m)	0.171	$d_s$ (m)	0.006
$H_{\text{bed}}$ (m)	0.08	$T_h$ ( $^{\circ}\text{C}$ )	650
$D_{\text{bed}}$ (m)	0.04	$T_c$ ( $^{\circ}\text{C}$ )	350
$\phi$ (-)	0.417	HTF	Air

In the present study, the DEM method is employed to generate 515 spheres (Bai et al., 2009). By using EDEM program, the solid spherical particles are fallen to the bottom of the tank by gravity. A balance is created for all the forces that affected the solid sphere during falling and solving, including the force of gravity, the force between spheres as well as the force between spheres and wall of the tank. The DEM simulation is stopped during the generation of solid spheres when the final state is reached, which means that the velocity of all spheres is approximately equal to zero.

## 2.2 Governing equations and computational methods

In this study, the fluid flow is unsteady and incompressible. The three-dimensional Navier-Stokes and energy equations are applied to show the fluid flow and temperature distributions during the charging/discharging cycles. The particle Reynolds number ( $Re_p$ ) is changing from 400 to 1,600 in this study, so, it is expected that the flow will be turbulent flow within the tank as reported in (Yang et al., 2010). The RNG k- $\epsilon$  turbulence model is recommended to study the turbulent flow in the porous medium, especially for small-scale eddies that are independent of larger phenomena (Yang et al., 2010). The RNG k- $\epsilon$  turbulence model and enhanced wall treatment are used in this study. The equations of conservation for mass, momentum, and energy are presented as:

Continuity:

$$\frac{\partial \rho}{\partial t} + \rho(\nabla \cdot \vec{V}) = 0 \quad (1)$$

Momentum:

$$\rho_f \left[ \frac{\partial \vec{V}}{\partial t} + (\vec{V} \cdot \nabla \vec{V}) \right] = \rho g - \nabla p + \nabla \cdot [(\mu_t + \mu_r)(\nabla \vec{V} + (\nabla \vec{V})^T)] \quad (2)$$

Energy:

$$\rho_f \left[ \frac{\partial T}{\partial t} + (\vec{V} \cdot \nabla T) \right] = \nabla \cdot \left[ \left( \frac{k_f}{c_p} + \frac{\mu_t}{\sigma_T} \right) \cdot (\nabla T) \right] \quad (3)$$

The RNG k- $\epsilon$  model transport equations are presented as:

$$k: \rho_f \left[ \frac{\partial k}{\partial t} + (\vec{V} \cdot \nabla k) \right] = \nabla \cdot \left[ \left( \mu_t + \frac{\mu_r}{\sigma_k} \right) \cdot \nabla k \right] + P_k - \rho_f \epsilon \quad (4)$$

$$\epsilon: \rho_f \left[ \frac{\partial \epsilon}{\partial t} + (\vec{V} \cdot \nabla \epsilon) \right] = \nabla \cdot \left[ \left( \mu_t + \frac{\mu_r}{\sigma_\epsilon} \right) \cdot \nabla \epsilon \right] + \frac{c_{\epsilon 1} \epsilon}{k} P_k - c_{\epsilon 2} \rho_f \frac{\epsilon^2}{k} \quad (5)$$

where  $P_k$  is the turbulence shear production,  $\mu_t$  is the turbulent viscosity,  $c_{\epsilon 1}$  and  $c_{\epsilon 2}$  are constants of the turbulence model in  $\epsilon$  equation,  $\sigma_T$ ,  $\sigma_k$  and  $\sigma_\epsilon$  are the Prandtl numbers in  $T$ ,  $k$  and  $\epsilon$  equations. The values of these constants are presented as:

$$P_k = \mu_t \cdot (\nabla \vec{V} + (\nabla \vec{V})^T) : \nabla \vec{V}; \quad \mu_t = \rho_f c_\mu \frac{k^2}{\epsilon} \quad (c_\mu = 0.085) \quad (6)$$

$$c_{\epsilon 1} = 1.42 - f_\eta \quad (f_\eta = \frac{\eta(1-\eta/4.38)}{1+0.012\eta^3}, \quad \eta = \frac{P_k}{\rho_f c_\mu \epsilon}) \quad (7)$$

where  $c_{\epsilon 2}$ ,  $\sigma_T$ ,  $\sigma_k$  and  $\sigma_\epsilon$  are equal 1.68, 1.0, 0.718, 0.718.

The commercial code of ANSYS FLUENT 16.0 is applied in this study to solve the continuity, momentum and energy equations. To couple the velocities and pressure in the equations of conservation, the SIMPLE algorithm is used. The second-order upwind scheme is applied to discretize the convective terms in the momentum, energy and turbulence equations. The residuals are adjusted for all the equations to be less than  $10^{-5}$  but, for energy equation, it is set to be less than  $10^{-8}$ .

## 2.3 Mesh generation and grid independence test

The geometry of the thermocline TES tank with 515 spheres is very complicated. In the present work, the geometric model is divided using tetrahedral mesh. Short cylinder bridges are created in order to modify the mesh at the points of contact. This modification is carried out according to a study conducted by (Dixon et al., 2012). It will be difficult to check the grid independence test for the thermocline TES tank with 515 spheres in the current study as the total number of the mesh elements will be greater than 45 M when mesh element size equal to 25 %  $d_s$ . For this reason, a thermocline TES tank with 70 spheres ( $H_{bed} = 0.08$  m,  $D_{bed}/d_s = 5$  and  $d_s = 0.008$  m) was created to determine the size of the appropriate computational element. The results showed that the grid size effect on the drag coefficient and the Nusselt number will be ineffective when the size of the computational element is less than  $1/20 d_s$ . The size of the computational element of  $1/20 d_s$  is selected for the current simulations.

## 3. Results and discussion

In the present work, the thermal behavior of the TES thermocline tank is one of the important parameters for determining the power generation and the STP efficiency. The process of thermal energy storage in the

thermocline tank keeps the STP plants in operation, the heat transfer process inside this tank during the charging/discharging cycles is of fundamental importance and will be studied in detail in this research.

### 3.1 Radial temperature distribution for charging/discharging cycles

Figures 2 and 3 show the HTF and spheres radial temperature distribution at different Reynolds number for charging process. Figure 2 is for the HTF and spheres radial temperature contours and Figure 3 is for HTF and spheres radial temperature profiles. During charging, the simulations show that the temperature of the fluid at the wall ( $r = 0.02$  m) rises faster than in the center of the bed ( $r = 0$ ) as shown in Figures 2 and 3. This is due to the wall channeling effect, as the velocity in the near wall region is higher than in the core region of the bed. The higher void fraction near the wall also results in a lower solid mass to absorb thermal energy. From Figure 2 and 3, it can be observed that the temperature rise occurs earlier when the Reynolds number increase. This can be mostly attributed to the increasing of driving force. At  $Re = 400$ , average temperature of core region for HTF and spheres are  $443.45$  °C and  $398.83$  °C, while in near-wall region for HTF and spheres are  $452.45$  °C and  $402.83$  °C. At  $Re = 800$ , average temperature of core region for HTF and spheres are  $477.63$  °C and  $454.27$  °C, while in near-wall region for HTF and spheres are  $482$  °C and  $456.8$  °C. At  $Re = 1,200$ , average temperature of core region for HTF and spheres are  $506.63$  °C and  $491.30$  °C, while in near-wall region for HTF and spheres are  $511.45$  °C and  $494$  °C. At  $Re = 1,600$ , average temperature of core region for HTF and spheres are  $528.82$  °C and  $518.19$  °C, while in near-wall region for HTF and spheres are  $532.84$  °C and  $521.34$  °C. The temperature in near-wall region is much higher than in core region at low Reynolds number but with increasing the Reynolds number this temperature difference decreasing.

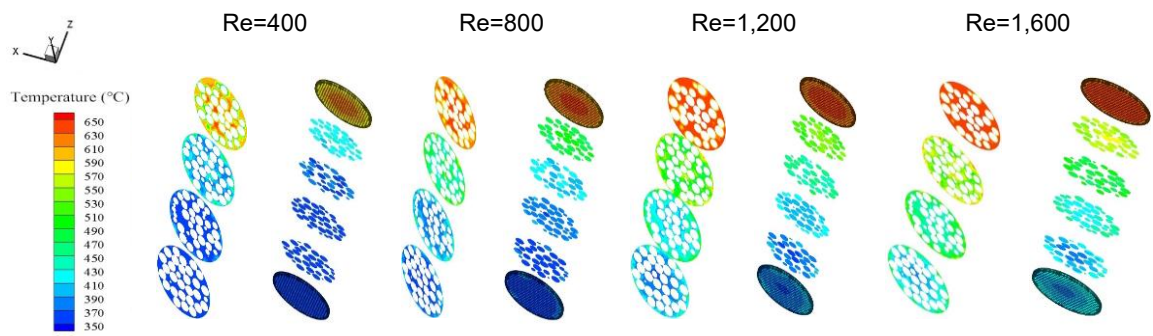


Figure 2: HTF and spheres radial temperature contours during charging cycle

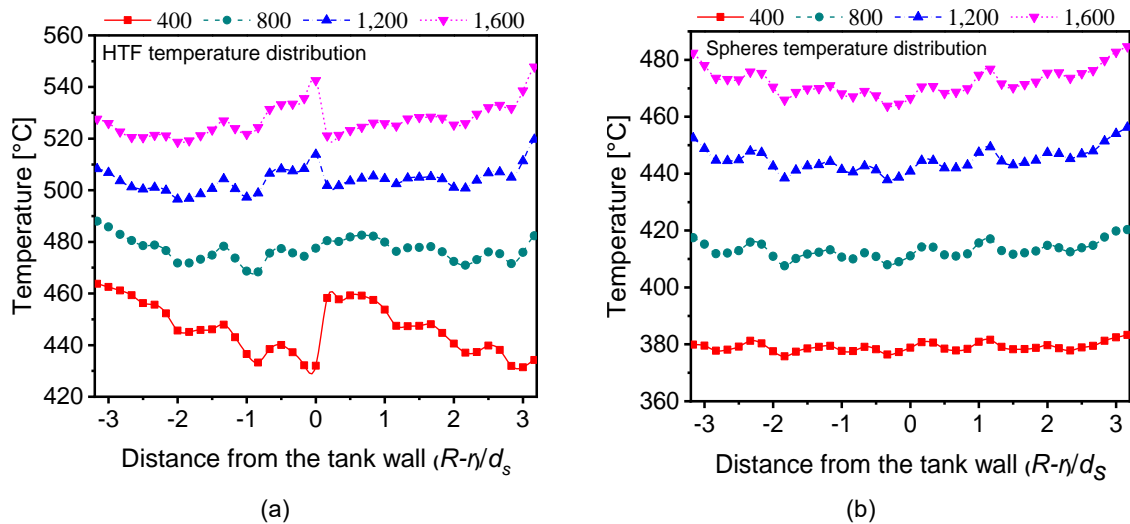


Figure 3: Radial temperature distribution during charging cycle for: (a) HTF and (b) Spheres

Figures 4 and 5 show the HTF and spheres radial temperature distribution at different Reynolds number for discharging process. Figure 4 is for the HTF and spheres radial temperature contours and Figure 5 is for HTF and spheres radial temperature profiles. As shown in Figures 4 and 5, in the discharging process, the temperature difference profiles present more complexity, resulting from not only the forced convection and the structure of the distributor, but also the residual temperature distribution from the discharging process. For the HTF flowing upwards, the hot HTF in the space between the distributor and the packed bed is mixed by the cold HTF and then pushed upwards, resulting in  $\Delta T$  decreasing noticeably at the beginning of the discharge process. Then as the front of cold HTF arrives, the  $\Delta T$  increase due to the higher velocity of the cold HTF near the wall. When the cold HTF mainstream arrives, the isotherms change gradually from convex to concave in the interior of the packed bed, and the temperature differences all decrease. For the cold HTF flowing upwards, the major difference in temperature difference profile occurs at the beginning of the discharging process, which has no the declining stage, resulting from the structure of the distributor. There is very little declining stage at the beginning of the discharging process and the rapid change of temperature difference appears much earlier in the HTF flowing discharging than charging. At  $Re = 400$ , average temperature of core region for HTF and spheres are  $583.53\text{ }^{\circ}\text{C}$  and  $622.55\text{ }^{\circ}\text{C}$ , while in near-wall region for HTF and spheres are  $580.6\text{ }^{\circ}\text{C}$  and  $618.13\text{ }^{\circ}\text{C}$ . At  $Re = 800$ , average temperature of core region for HTF and spheres are  $572.82\text{ }^{\circ}\text{C}$  and  $589.62\text{ }^{\circ}\text{C}$ , while in near-wall region for HTF and spheres are  $566.6\text{ }^{\circ}\text{C}$  and  $582.50\text{ }^{\circ}\text{C}$ . At  $Re = 1,200$ , average temperature of core region for HTF and spheres are  $547.79\text{ }^{\circ}\text{C}$  and  $558.79\text{ }^{\circ}\text{C}$ , while in near-wall region for HTF and spheres are  $540.27\text{ }^{\circ}\text{C}$  and  $550.92\text{ }^{\circ}\text{C}$ . At  $Re = 1,600$ , the average temperature of core region for HTF and spheres are  $523.45\text{ }^{\circ}\text{C}$  and  $531.75\text{ }^{\circ}\text{C}$ , while in near-wall region for HTF and spheres are  $515.16\text{ }^{\circ}\text{C}$  and  $523.36\text{ }^{\circ}\text{C}$ . The temperature in near-wall region is much lower than in core region due to the wall effect.

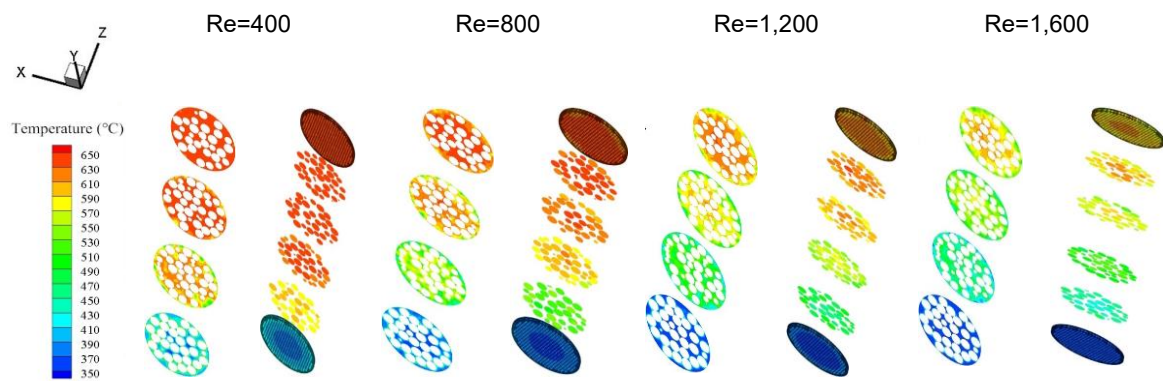


Figure 4: HTF and spheres radial temperature contours during discharging cycle

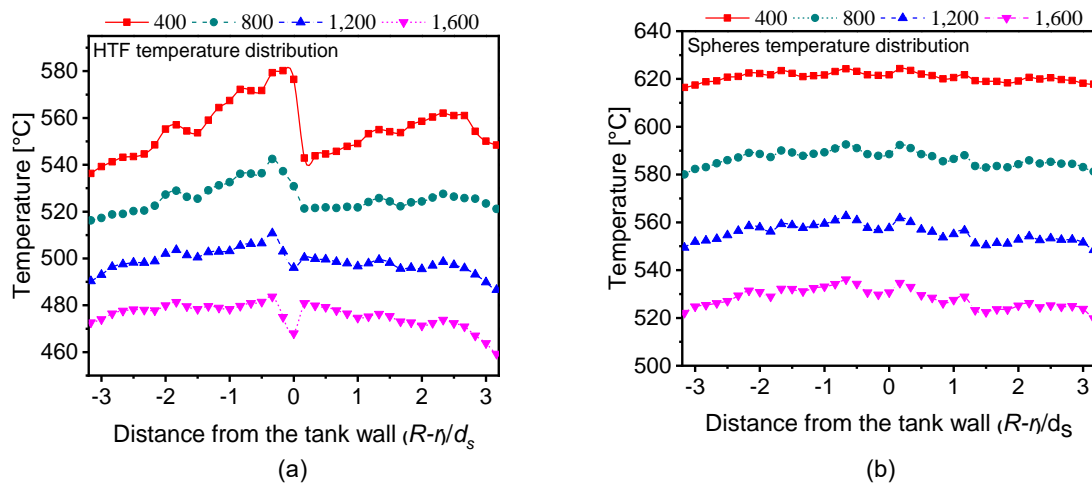


Figure 5: Radial temperature distribution during discharging cycle for: (a) HTF and (b) Spheres

#### 4. Conclusions

In the present work, the DEM coupled with the CFD are adopted to study the fluid flow and heat transfer process of an air rock thermocline TES tank prototype. The study is carried out to investigate the thermal behaviour of the TES thermocline tank by changing the Reynolds number. The results demonstrated that the higher void fraction near the wall results in a lower solid mass to absorb thermal energy and the temperature in the near-wall region is much higher than in core region at low Reynolds number but with increasing the Reynolds number this temperature difference decreasing. Also, the results show that the temperature difference between both the HTF and the spheres for charging cycle decreases with increasing of the Reynolds number, but also the total rate of heat transfer increases. The results illustrated that the difference in temperature between both the spheres and the HTF during the discharging cycle decreases with increase in the Reynolds number and this difference in temperature is less during the discharging cycle than the charging cycle. This work can be extended by investigating the charging/discharging efficiency, overall efficiency, capacity ratio, and utilization ratio of the air rock thermocline thermal energy storage tank to optimize its thermal performance which used in solar tower power plants

#### Acknowledgments

This work is financially supported by the Foundation for Innovative Research Groups of the National Natural Science Foundation of China (No.51721004) and the 111 Project (B16038).

#### References

- Bai H., Theuerkauf J., Gillis P.A., Witt P.M., 2009, A coupled DEM and CFD simulation of flow field and pressure drop in fixed bed reactor with randomly packed catalyst particles, *Industrial & Engineering Chemistry Research*, 48, 4060-4074.
- Cocco D., Serra F., 2015, Performance comparison of two-tank direct and thermocline thermal energy storage systems for 1 MWe class concentrating solar power plants, *Energy*, 81, 526-536.
- Dixon A.G., Walls G., Stanness H., Nijemeisland M., Stitt E.H., 2012, Experimental validation of high Reynolds number CFD simulations of heat transfer in a pilot-scale fixed bed tube, *Chemical Engineering Journal*, 200, 344-356.
- Elfeky K.E., Ahmed N., Wang Q., 2018, Numerical comparison between single PCM and multi-stage PCM based high temperature thermal energy storage for CSP tower plants, *Applied Thermal Engineering*, 139, 609-622.
- Hänchen M., Brückner S., Steinfeld A., 2011, High-temperature thermal storage using a packed bed of rocks-heat transfer analysis and experimental validation, *Applied Thermal Engineering*, 31, 1798-1806.
- Hoivik N., Greiner C., Barragan J., Iniesta A.C., Skeie G., Bergan P., Blanco-Rodriguez P., Calvet N., 2019, Long-term performance results of concrete-based modular thermal energy storage system, *Journal Energy Storage*, 24, 100735.
- Li B., Ju F., 2018, Thermal stability of granite for high temperature thermal energy storage in concentrating solar power plants, *Applied Thermal Engineering*, 138, 409-416.
- Löf G.O.G., Hawley R.W., 1948, Unsteady-state heat transfer between air and loose solids, *Industrial Chemical Engineering*, 40, 1061-1070.
- Pizzolato A., Donato F., Verda V., Santarelli M., Sciacovelli A., 2017, CSP plants with thermocline thermal energy storage and integrated steam generator—Techno-economic modeling and design optimization, *Energy*, 139, 231-246.
- Pramanik S., Ravikrishna R.V., 2017, A review of concentrated solar power hybrid technologies, *Applied Thermal Engineering*, 127, 602-637.
- Rao C.R.C., Vigneshwaran K., Niyas H., Muthukumar P., 2019, Performance investigation of lab-scale sensible heat storage prototypes, *International Journal of Green Energy*, 16, 1363-1378.
- Tiskatine R., Aharoune A., Bouirden L., Ihlal A., 2017, Identification of suitable storage materials for solar thermal power plant using selection methodology, *Applied Thermal Engineering*, 117, 591-608.
- Yang J., Wang Q., Zeng M., Nakayama A., 2010, Computational study of forced convective heat transfer in structured packed beds with spherical or ellipsoidal particles, *Chemical Engineering Science*, 65, 726-738.
- Zanganah G., Khanna R., Walser C., Pedretti A., Haselbacher A., Steinfeld A., 2015, Experimental and numerical investigation of combined sensible–latent heat for thermal energy storage at 575 °C and above, *Solar Energy*, 114, 77-90.